arXiv:1511.03365v1 [cond-mat.str-el] 11 Nov 2015

Photoinduced demagnetization and insulator-to-metal transition in ferromagnetic insulating $BaFeO_3$ thin films

T. Tsuyama,[1,2] S. Chakraverty,[3,4] N. Pontius,[5] C. Schüßler-Langeheine,[5]
H. Y. Hwang,[3,6,7] Y. Tokura,[2,3] and H. Wadati[1,2,*]

[1]*Institute for Solid State Physics, University of Tokyo, Kashiwanoha 5-1-5, Chiba 277-8581, Japan*
[2]*Department of Applied Physics and Quantum-Phase Electronics Center (QPEC), University of Tokyo, Hongo, Tokyo 113-8656, Japan*
[3]*RIKEN Center for Emergent Matter Science (CEMS), Wako, Saitama 351-0198, Japan*
[4]*Institute of Nano Science and Technology, Phase - 10, Sector - 64, Mohali, Punjab, India*
[5]*Helmholtz-Zentrum Berlin für Materialien und Energie GmbH, Albert-Einstein-Straße 15, 12489 Berlin, Germany*
[6]*Stanford Institute for Materials and Energy Sciences, SLAC National Accelerator Laboratory, Menlo Park, CA 94025, USA*
[7]*Department of Applied Physics, Stanford University, Stanford, CA 94305, USA*

(Dated: November 12, 2015)

We studied the electronic and magnetic dynamics of ferromagnetic insulating $BaFeO_3$ thin films by using pump-probe time-resolved resonant x-ray reflectivity at the Fe $2p$ edge. By changing the excitation density, we found two distinctly different types of demagnetization with a clear threshold behavior. We assigned the demagnetization change from slow ($\sim$ 150 ps) to fast ($<$ 70 ps) to a transition into a metallic state induced by laser excitation. These results provide a novel approach for locally tuning magnetic dynamics. In analogy to heat assisted magnetic recording, metallization can locally tune the susceptibility for magnetic manipulation, allowing to spatially encode magnetic information.

PACS numbers: 71.30.+h, 73.61.-r, 75.70.-i, 78.66.-w

Control of magnetic states by optical excitations in magnetically ordered materials has attracted considerable attention since the demonstration of ultrafast demagnetization in Ni within 1 ps, explored by time-resolved magneto-optical Kerr effect studies [1]. Ultrafast demagnetization was also observed for other elementary ferromagnetic transition metals such as Co and Fe, and intermetallic alloys [2, 3].

Several mechanisms have been proposed to understand the ultrafast demagnetization. Beaurepaire *et al.* proposed a phenomenological "three-temperature model" in order to understand the ultrafast demagnetization of Ni, which considers three interacting reservoirs of electrons, spins, and lattice, and suggested the importance of direct electron-spin interactions. Since the electron, spin, and lattice systems are quite tightly coupled to each other in strongly correlated $3d$ transition metal oxides, it is interesting to investigate the photoinduced dynamics with respect to the electronic states and magnetism [4–15].

For this study, we chose fully oxidized single crystalline $BaFeO_3$ thin films, which show unusual behaviors of ferromagnetic and insulating properties with saturation magnetization and Curie temperature of 3.2 μ_B/formula unit and 115 K, respectively [16]. The large magnetic moment of $BaFeO_3$ thin films results in quite large peak intensity of Fe $2p$ x-ray magnetic circular dichroism (XMCD), $\sim$ 18 % of the x-ray absorption peak intensity [17]. Thus, $BaFeO_3$ thin films are appropriate samples to carry out time-resolved magnetic circular dichroism experiments. Furthermore, the investigation of the demagnetization dynamics of insulators allows one to relate electronic structure to magnetic dynamics.

In order to investigate the magnetic dynamics of ferromagnetic insulating $BaFeO_3$ thin films, we performed time-resolved reflectivity studies at the Femtospex slicing facility at the synchrotron radiation source BESSY II [18], using circularly polarized x-ray pulses. Our experimental method has the advantage that, in one reflectivity experiment, we can probe electronic structure as well as magnetism. $BaFeO_{2.5}$ thin films were grown on $SrTiO_3$ (001) substrate with the film thickness of 50 nm, using pulsed laser deposition [16]. After the deposition, $BaFeO_{2.5}$ thin films were annealed at 200 °C under ozone atmosphere to obtain $BaFeO_3$ thin films [16]. The quality of the thin-film samples were confirmed by x-ray diffraction, Fe $2p$ x-ray absorption spectroscopy, and Fe $2p$ core-level hard x-ray photoemission spectroscopy measurements by comparing cluster-model calculations, which found that the formal valence of Fe was 4+ [16, 17]. The experimental geometry is shown schematically in Fig. 1 (a). We used fixed circular polarization and created magnetic contrast by switching the direction of the magnetic field (H), which was oriented along the sample surface ([010] direction). We recorded specular reflectivity data for two magnetization directions, R^+ and R^-. The average reflectivity $R = (R^+ + R^-)/2$ is a measure of the electronic and structural properties, while the magnetic circular dichroism in reflectivity (MCDR) sig-

*Electronic address: wadati@issp.u-tokyo.ac.jp; URL: http://www.geocities.jp/qxbqd097/index2.htm

nal $DR = (R^+ - R^-)/2$ is a measure of the sample magnetization [19]. A Ti-Sapphire laser ($\lambda = 800$ nm, $h\nu = 1.55$ eV) with the pulse width of ~ 50 fs was employed as a pump laser with π polarization. The spot size of the pump laser was ~ 0.40 mm (horizontal) $\times$ 0.25 mm (vertical), and that of the probe x-ray was ~ 0.1 mm $\times$ 0.1 mm. The repetition rate of the time-resolved measurement was 3 kHz, limited by the frequencies of the pump laser. The pumped and unpumped signals were obtained alternatively. The time resolution was 70 ps, corresponding to the pulse length of the probe x-ray.

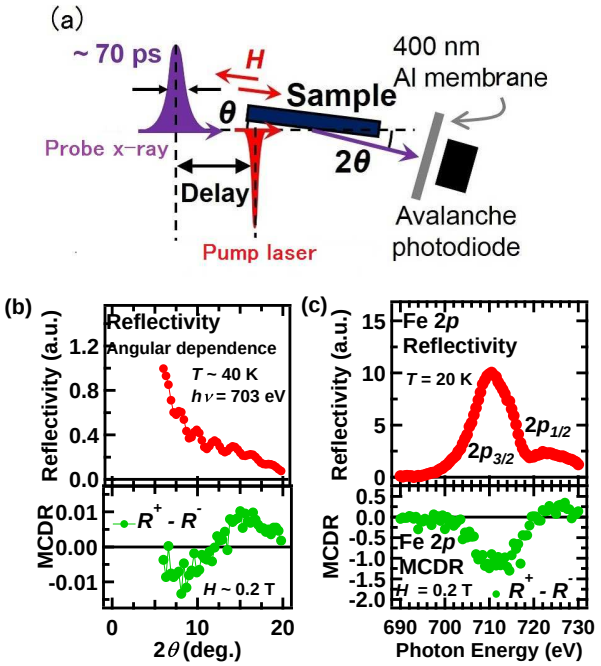

FIG. 1: (a) Geometry of the measurements. Panel (b) shows the reflectivity (top) and MCDR (bottom) intensity from $BaFeO_3$ thin films as a function of 2θ. Panel (c) shows the photon energy dependence of reflectivity (top) and MCDR (bottom).

The angular dependences of reflectivity and MCDR are shown in Fig. 1 (b) for a photon energy of 703 eV. The angular dependence of reflectivity show oscillating structures, attributed to the interference between x-rays reflected from the surface and interface of the thin-film sample. It enables us to estimate the film thickness of the sample to be (48 ± 1) nm, in good agreement with the evaluation of $\sim (50 \pm 1)$ nm by reflection high-energy electron diffraction. The oscillating structures in the angular dependence of reflectivity also imply a probing depth larger than the film thickness. MCDR also shows an angular dependence with sign reversal as shown in Fig. 1 (b). We fixed 2θ to be $\sim 15°$, which maximizes the MCDR to about 12 % of the average reflectivity. Figure 1 (c) shows the photon-energy dependence of reflectivity and MCDR. Although the photon-energy dependence of MCDR is different from the circular dichroism obtained from x-ray absorption spectra [17], it is a suited measure of the sample magnetization [19]. We fixed the photon energy to be $h\nu = 714$ eV, and the time evolution of the intensities of reflectivity as well as XMCD at this photon energy are traced in order to investigate the electronic and magnetic dynamics of $BaFeO_3$ thin films.

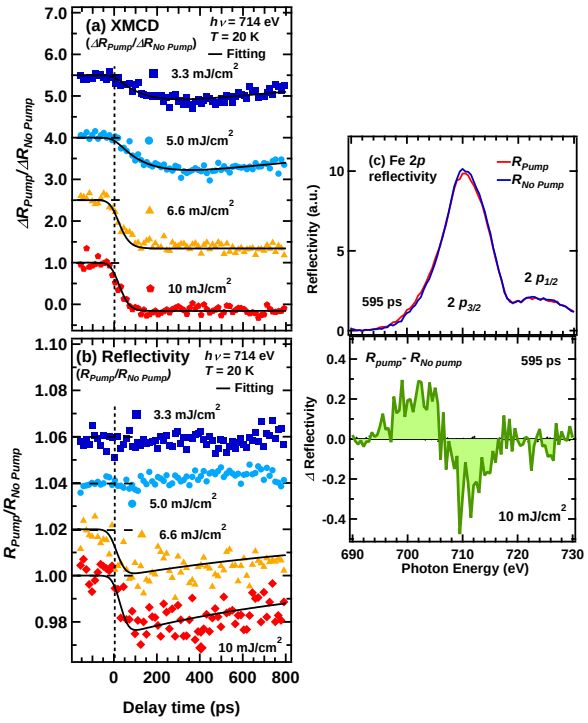

FIG. 2: Time evolution of (a) XMCD intensity and (b) reflectivity of $BaFeO_3$ thin films for various pump laser fluence. All the curves, except for the case of 10 mJ/cm^2, are shifted upward for clarity. (c) The reflectivity spectra with and without the pump effect (top). The difference of the spectra (bottom).

Figure 2 (a) shows the time evolution of the MCDR intensities for different pump fluence. The vertical axis shows the excited MCDR intensities normalized by the unpumped signal (*i.e.* $\Delta R_{Pump}/\Delta R_{NoPump}$). Here, the subscript of Pump and No Pump denote the signals with and without the laser excitations, respectively. The MCDR intensities decrease after the incidence of the pump laser at $t = 0$. The time evolution of the MCDR intensity show different behaviors with the change of the pump fluence (F). When F is smaller than 5.0 mJ/cm^2, the demagnetization time is relatively slow and magnetization recovery sets in after about 400 ps. When the pump F is larger than 6.6 mJ/cm^2, on the other hand, the demagnetization time is quite fast and no recovery of the magnetization can be observed within the first 800 ps. We assign the different behavior of the demagnetization dynamics to a laser-induced insulator-to-metal transitions for $F \geq 6.6$ mJ/cm^2, as discussed in the following.

We show the time evolution of the intensity of the av-

erage reflectivity in Fig. 2 (b), which allows us to investigate the electronic dynamics. The vertical axis shows the excited reflectivity intensities normalized by those without excitation (*i.e.* R_{Pump}/R_{NoPump}). No pump effects were observed for $F \leq 5.0$ mJ/cm^2 with our time resolution of 70 ps. Pump effects, on the other hand, were clearly observed for $F \geq 6.6$ mJ/cm^2. They occur via a transfer of spectral weight from the maximum of the Fe $2p_{3/2}$ resonance (710 eV) towards lower excitation energies as evidenced by comparing the spectra with and without laser in Fig. 2 (c). The transfer to lower energies is particularly evident in the difference plot in the lower frame. A similar behavior with spectral weight transfers above a fluence threshold was observed in time-resolved x-ray absorption spectroscopy from VO_2 [6] and interpreted as a laser induced insulator-to-metal transition. Since $BaFeO_3$ thin films are near the phase boundary of a metal-insulator transition, we assign the spectral weight transfer in this material to a similar mechanism.

In order to discuss the results quantitatively, we fitted them using exponential functions for decay and recovery (solid lines in Fig. 2 (a) and (b)); τ_{decay} and $\tau_{recovery}$ denote the corresponding time constants. To take temporal resolution into account, the fitting function was convoluted by a Gaussian with a full width at half maximum of $\tau_{reso} = 70$ ps. The parameters extracted from the experimental delay scans are summarized in TABLE I.

TABLE I: Fitting parameters of the time evolution of MCDR and reflectivity intensity in Fig. 2. We fixed $\tau_{reso} = 70$ ps.

F [mJ/cm^2]	$\tau_{decay,MCDR}$ [ps]	$\tau_{recovery,MCDR}$ [ps]	$\tau_{decay,ref}$ [ps]	$\tau_{recovery,ref}$ [ps]
3.3	140	1000	–	–
5.0	150	1200	–	–
6.6	29	–	16	1200
10	23	–	9.0	1000

The quantitative analysis confirms the existence of two different kinds of dynamics for high and low fluences respectively. We show the demagnetization time, τ_{decay} determined by the fitting functions in the top panel of Fig. 3. The demagnetization time is estimated to be $\tau_{decay} \sim 150$ ps for the weaker excitations ($F \leq 5.0$ mJ/cm^2), and demagnetization faster than our temporal resolution was observed for the strong pump fluence ($F \geq 6.6$ mJ/cm^2). In the bottom panel of Fig. 3, we show the amplitude of the reflectivity change, which is a measure of the spectral weight transfer indicative of the insulator-to-metal transition, as a function of laser fluence. From the clear threshold behavior of this quantity we deduce that a sufficiently high density of excited carriers reduces electron-electron and electron-phonon interactions, which are the origins of the insulating properties in $BaFeO_3$ thin films [16, 17].

We then conclude that the drastic changes of in the

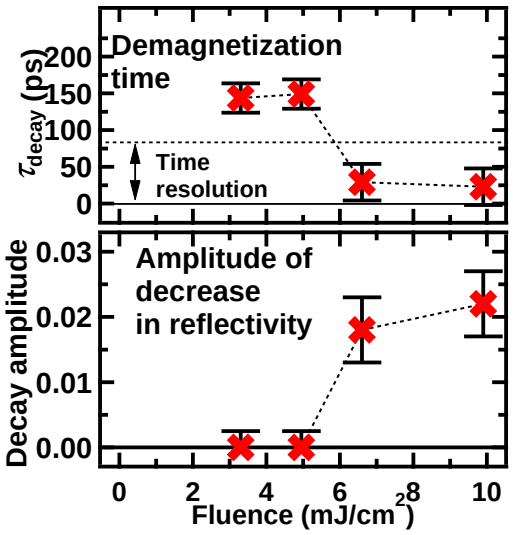

FIG. 3: The demagnetization time τ_{decay} (top), determined from Fig. 2, and the magnitude of decay of reflectivity due to the pump (bottom) are shown.

demagnetization dynamics with laser fluence are due to the photoinduced insulator-to-metal transition as shown by the time-resolved reflectivity measurement, since the electronic structure significantly influences the demagnetization dynamics [2, 5, 8, 9]. Half metals and ferromagnetic insulators usually show relatively slow demagnetization in the range of from 100 ps to 1000 ps, while itinerant ferromagnets (with low spin polarization) can show ultrafast demagnetization [2, 5, 8, 9]. Within common models for ultrafast magnetic dynamics, these differences in demagnetization dynamics are explained by the differences of strength of coupling between electronic and spin reservoirs. Ferromagnetic metals with low spin polarization, such as Ni and Fe, have strong coupling between electron and spin reservoirs because the electronic structure of ferromagnetic metals can accommodate spin-flip excitations with quasiparticle scatterings, resulting in the ultrafast demagnetization due to the rapid increase of spin temperature via the electron reservoir. Half metals and ferromagnetic insulators, on the other hand, do not have strong coupling between the reservoirs. This is because the spin-flip excitations are significantly suppressed after the rapid increase of electron temperature in their electronic structure, resulting in slow increase of spin temperature via heating of the lattice.

Since undisturbed $BaFeO_3$ thin films are ferromagnetic insulators, the spin scattering after the electronic excitations should be suppressed. The slow demagnetization time of ~ 150 ps in $BaFeO_3$ thin films with small pump fluence ($F \leq 5.0$ mJ/cm^2) can be explained by heating via the lattice. The large pump fluence ($F \geq 6.6$ mJ/cm^2), however, induces an insulator-to-metal transition in $BaFeO_3$ thin films quite rapidly, which results in the unusually fast demagnetization in $BaFeO_3$ thin films

for a ferromagnetic insulator.

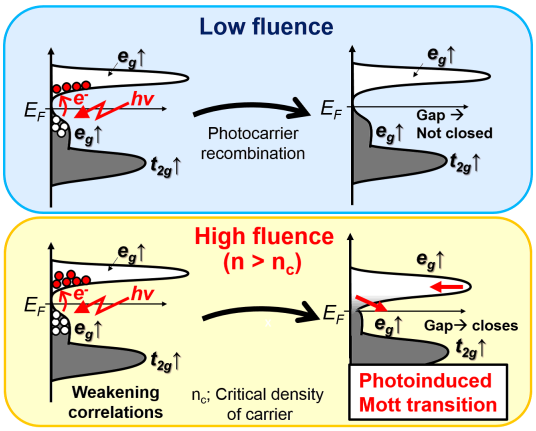

FIG. 4: Mechanism of insulator-to-metal transition induced by the strong laser excitation.

When the pump fluence is weaker than 5.0 mJ/cm^2, magnetizations in $BaFeO_3$ thin films recover with the time constant of $\tau_{recovery} \sim 1000$ ps. The time scale of ~ 1000 ps can be assigned to heat diffusion needed to cool the sample below the magnetic ordering temperature after electron, lattice, and spin systems have reached thermal equilibrium. Remarkably, the time-resolved reflectivity change for strong pump fluence also shows a recovery on this time scale of $\tau_{recovery} \sim 1000$ ps, indicating that also here heat diffusion is the relevant mechanism. This latter observation is quite notable, because equilibrium between the electron and lattice temperature should be reached within 1 ps. The slow reopening of the band-gap on time scales of ~ 1000 ps shows that for high excitation densities we drive the system into a metastable state. As a mechanism for the long life time of the metallic state, we consider that hot carriers, generated by the quasiparticle scattering and closing the band gap, prevent it from opening again by reducing electron-electron and electron-phonon interactions [11]. This process is schematically shown in Fig. 4.

In conclusion, we investigated the electronic and magnetic dynamics by time-resolved reflectivity and MCDR measurement on $BaFeO_3$ thin films. When the pump laser fluence is smaller than 5.0 mJ/cm^2, relatively slow demagnetization of $\tau_{decay} \sim 150$ ps was observed, due to the insulating properties of the ground state in $BaFeO_3$ thin films without any changes in Fe $2p$ x-ray reflectivity. When the pump laser fluence is stronger than 6.6 mJ/cm^2, on the other hand, rapid changes in Fe $2p$ x-ray reflectivity are observed, which is attributed to a transition into a metallic state, resulting in an unusually fast demagnetization with $\tau_{decay} < 70$ ps. Since $BaFeO_3$ thin films are near the phase boundary of a metal-insulator transition, the insulating phase is quite sensitive to carrier density. Thus, the origin of the insulator-to-metal transition is a photoinduced Mott transition into a metastable state stabilized by screened electron-electron and electron-phonon interactions. Our findings indicate a mechanism for tuning magnetic dynamics in correlated materials, which resembles heat-assisted magnetic switching in metallic magnets. By creating a sufficiently high excitation density, spin flip scattering channels open up which increase the spin systems susceptibility to external manipulation.

This research was supported by the Japan Society the Promotion of Science (JSPS) through the Funding Program for World-Learning Innovative R&D on Science and Technology (FIRST program), JSPS Giant-in-Aid for Scientific Research, and by Grant for Basic Science Research Projects from the Sumitomo Foundation. This work was also partially supported by the Ministry of Education, Culture, Sports, Science and Technology of Japan (X-ray Free Electron Laser Priority Strategy Program). H. Y. H. acknowledges support by the Department of Energy, Basic Energy Sciences, Materials Science and Engineering Division, under Contract No. DE-AC02-76SF00515.

[1] E. Beaurepaire, J.-C. Merle, A. Daunois, and J.-Y. Bigot, Phys. Rev. Lett. **76**, 4250 (1996).
[2] A. Kirilyuk, A. V. Kimel, and T. Rasing, Rev. Mod. Phys. **82**, 2731 (2010).
[3] J. Stöhr and H. C. Siegmann, *Magnetism* (Springer, Berlin, 2006).
[4] K. Miyano, T. Tanaka, Y. Tomioka, and Y. Tokura, Phys. Rev. Lett. **78**, 4257 (1997).
[5] T. Kise, T. Ogasawara, M. Ashida, Y. Tomioka, Y. Tokura, and M. Kuwata-Gonokami, Phys. Rev. Lett. **85**, 1986 (2000).
[6] A. Cavalleri, M. Rini, H. H. W. Chong, S. Fourmaux, T. E. Glover, P. A. Heimann, J. C. Kieffer, and R. W. Schoenlein, Phys. Rev. Lett. **95**, 067405 (2005).
[7] T. Ogasawara, K. Ohgushi, Y. Tomioka, K. S. Takahashi, H. Okamoto, M. Kawasaki, and Y. Tokura, Phys. Rev. Lett. **94**, 087202 (2005).
[8] Q. Zhang, A. V. Nurmikko, G. X. Miao, G. Xiao, and A. Gupta, Phys. Rev. B **74**, 064414 (2006).
[9] G. M. Muller, J. Walowski, M. Djordjevic, G.-X. Miao, A. Gupta, A. V Ramos, K. Gehrke, V. Moshnyaga, K. Samwer, J. Schmalhorst, A. Thomas, A. Hatten, G. Reiss, J. S. Moodera, and M. Monzenberg, Nat. Mater. **8**, 56 (2009).
[10] B. Koopmans, G. Malinowski, F. Dalla Longa, D. Steiauf, M. Fahnle, T. Roth, M. Cinchetti, and M. Aeschlimann, Nat. Mater. **9**, 259 (2010).
[11] H. Okamoto, T. Miyagoe, K. Kobayashi, H. Uemura, H. Nishioka, H. Matsuzaki, A. Sawa, and Y. Tokura, Phys. Rev. B **83**, 125102 (2011).
[12] I. Radu, K. Vahaplar, C. Stamm, T. Kachel, N. Pontius, H. A. Durr, T. A. Ostler, J. Barker, R. F. L. Evans, R.

W. Chantrell, A. Tsukamoto, A. Itoh, A. Kirilyuk, T. Rasing, and A. V. Kimel, Nature **472**, 205 (2011).

[13] S. de Jong, R. Kukreja, C. Trabant, N. Pontius, C. F. Chang, T. Kachel, M. Beye, F. Sorgenfrei, C. H. Back, B. Bräuer, W. F. Schlotter, J. J. Turner, O. Krupin, M. Doehler, D. Zhu, M. A. Hossain, A. O. Scherz, D. Fausti, F. Novelli, M. Esposito, W. S. Lee, Y. D. Chuang, D. H. Lu, R. G. Moore, M. Yi, M. Trigo, P. Kirchmann, L. Pathey, M. S. Golden, M. Buchholz, P. Metcalf, F. Parmigiani, W. Wurth, A. Fohlisch, C. Schüßler-Langeheine, and H. A. Dürr, Nat. Mater. **12**, 882 (2013).

[14] N. Bergeard, V. Lopez-Flores, V. Halt, M. Hehn, C. Stamm, N. Pontius, E. Beaurepaire, and C. Boeglin, Nat. Commun. **5**, 3466 (2014).

[15] P. Beaud, A. Caviezel, S. O. Mariager, L. Rettig, G. Ingold, C. Dornes, S.-W. Huang, J. A. Johnson, M. Radovic, T. Huber, T. Kubacka, A. Ferrer, H. T. Lemke, M. Chollet, D. Zhu, J. M. Glownia, M. Sikorski, A. Robert, H. Wadati, M. Nakamura, M. Kawasaki, Y. Tokura, S. L. Johnson, and U. Staub, Nat. Mater. **13**, 923 (2014).

[16] S. Chakraverty, T. Matsuda, N. Ogawa, H. Wadati, E. Ikenaga, M. Kawasaki, Y. Tokura, and H. Y. Hwang, Appl. Phys. Lett. **103**, 142416 (2013).

[17] T. Tsuyama, T. Matsuda, S. Chakraverty, J. Okamoto, E. Ikenaga, A. Tanaka, T. Mizokawa, H. Y. Hwang, Y. Tokura, and H. Wadati, Phys. Rev. B **91**, 115101 (2015).

[18] K. Holldack, J. Bahrdt, A. Balzer, U. Bovensiepen, M. Brzhezinskaya, A. Erko, A. Eschenlohr, R. Follath, A. Firsov, W. Frentrup, L. Le Guyader, T. Kachel, P. Kuske, R. Mitzner, R. Muller, N. Pontius, T. Quast, I. Radu, J.-S. Schmidt, C. Schüßler-Langeheine, M. Sperling, C. Stamm, C. Trabant and A. Fohlisch, J. Synchrotron Rad. **21**, 1090 (2014).

[19] H.-Ch. Mertins, D. Abramsohn, A. Gaupp, F. Schafers, W. Gudat, O. Zaharko, H. Grimmer, and P. M. Oppeneer, Phys. Rev. B **66**, 184404 (2002).